Clim. Past, 16, 1999–2015, 2020
https://doi.org/10.5194/cp-16-1999-2020

Climate of the Past
Open Access
EGU

Glacial history of Inglefield Land, north Greenland from combined in situ ^{10}Be and ^{14}C exposure dating

Anne Sofie Søndergaard[1], Nicolaj Krog Larsen[1,2], Olivia Steinemann[3], Jesper Olsen[4], Svend Funder[2], David Lundbek Egholm[1], and Kurt Henrik Kjær[2]

[1]Department of Geoscience, Aarhus University, Høegh Guldbergs Gade 2, 8000 Aarhus C, Denmark
[2]Globe Institute, University of Copenhagen, Øster Voldgade 5-7, 1350 Copenhagen K, Denmark
[3]Department of Physics, Institute for Particle Physics and Astrophysics, ETH Zürich, Otto-Stern-Weg 5, 8093 Zürich, Switzerland
[4]Department of Physics and Astronomy, Aarhus University, Ny Munkegade 120, 8000 Aarhus C, Denmark

Correspondence: Anne Sofie Søndergaard (annesofie@geo.au.dk)

Received: 2 May 2020 – Discussion started: 6 May 2020
Revised: 25 August 2020 – Accepted: 22 September 2020 – Published: 30 October 2020

Abstract. Determining the sensitivity of the Greenland Ice Sheet (GrIS) to Holocene climate changes is a key prerequisite for understanding the future response of the ice sheet to global warming. In this study, we present new information on the Holocene glacial history of the GrIS in Inglefield Land, north Greenland. We use ^{10}Be and in situ ^{14}C exposure dating to constrain the timing of deglaciation in the area and radiocarbon dating of reworked molluscs and wood fragments to constrain when the ice sheet retreated behind its present-day extent. The ^{10}Be ages are scattered ranging from ca. 92.7 to 6.8 ka, whereas the in situ ^{14}C ages range from ca. 14.2 to 6.7 ka. Almost half of the apparent ^{10}Be ages predate the Last Glacial Maximum and up to 89 % are to some degree affected by nuclide inheritance. Based on the few reliable ^{10}Be ages, the in situ ^{14}C ages and existing radiocarbon ages from Inglefield Land, we find that the deglaciation along the coast commenced at ca. 8.6–8.3 ka cal BP in the western part and ca. 7.9 ka in the central part, following the opening of Nares Strait and arrival of warm waters. The ice margin reached its present-day position at ca. 8.2 ka at the Humboldt Glacier and ca. 6.7 ka in the central part of Inglefield Land. Radiocarbon ages of reworked molluscs and wood fragments show that the ice margin was behind its present-day extent from ca. 5.8 to 0.5 ka cal BP. After 0.5 ka cal BP, the ice advanced towards its Little Ice Age position. Our results emphasize that the slowly eroding and possibly cold-based ice in north Greenland makes it difficult to constrain the deglaciation history based on ^{10}Be ages alone unless they are paired with in situ ^{14}C ages. Further, combining our findings with those of recently published studies reveals distinct differences between deglaciation patterns of northwest and north Greenland. Deglaciation of the land areas in northwest Greenland occurred earlier than in north Greenland, and periods of restricted ice extent were longer, spanning the Middle and Late Holocene. Overall, this highlights past ice sheet sensitivity to Holocene climate changes in an area where little information was available just a few years ago.

1 Introduction

Information about the glacial history of the Greenland Ice Sheet (GrIS) is important to constrain its sensitivity to past and ongoing climate changes (Lecavalier et al., 2017; Larsen et al., 2018). Since the 1990s, mass loss from the GrIS has accelerated, coinciding with atmospheric warming, and the ice sheet appears to be extremely sensitive to this warming, especially in north Greenland, where the ablation area has expanded by 46 % (Khan et al., 2015; Noël et al., 2019). As a result, the relative contribution to sea level rise from the north GrIS has increased significantly, primarily through enhanced runoff as well as ice discharge via calving and melting at the Humboldt Glacier front (Mouginot et al., 2019; Noël et al., 2019).

With the introduction of cosmogenic nuclide exposure dating, previously glaciated areas of Greenland have been systematically targeted, and > 1000 ^{10}Be exposure ages have been published within the last two decades (Sinclair et al., 2016).

In consequence, the late glacial and Holocene glaciation history is well constrained in most areas of Greenland (Bennike and Björck, 2002; Funder et al., 2011; Sinclair et al., 2016). However, there are still areas where the deglaciation chronology is constrained by minimum limiting radiocarbon ages of mainly marine molluscs along the coast and where inland exposure ages are unavailable (Bennike and Björck, 2002; Funder et al., 2011). This is particularly true for north Greenland including Inglefield Land where the current knowledge is primarily based on studies from late 1960s and 1970s (Nichols, 1969; Tedrow, 1970).

Despite that, ^{10}Be exposure dating has been shown to be an efficient tool for constraining the deglaciation of the GrIS, but the use of this method is not without pitfalls. The method assumes that the measured ^{10}Be concentration was produced in one single post-glacial exposure period, but a number of studies have demonstrated that this assumption does not always hold. A particular challenge arises when subglacial bedrock erosion is too slow to remove ^{10}Be inventories produced during earlier exposure periods, such as the previous interglacial. In such cases, the resulting age is typically referred to as an *apparent ^{10}Be exposure age* in acknowledgement of the fact that this age typically exceeds the true exposure age (Kelly et al., 2008; Corbett et al., 2015; Farnsworth et al., 2018; Larsen et al., 2018; Søndergaard et al., 2019; Ceperley et al., 2020; Skov et al., 2020). This problem of ^{10}Be nuclide inheritance emphasizes the need for new methods to be implemented in order to thoroughly constrain the glacial history in parts of Greenland where the ice is cold-based and inefficient erosion leads to widespread nuclide inheritance.

Here we use a combination of ^{10}Be and in situ ^{14}C exposure dating of boulders and pebbles to overcome the problem of nuclide inheritance and constrain the Holocene deglaciation history of the GrIS in Inglefield Land, north Greenland. In addition, we use radiocarbon dating of reworked marine molluscs and wood fragments to constrain the Holocene timing of restricted ice extent in the study area. Finally, we review and assess the glacial history in northwest and north Greenland with both local and regional climate records in order to expand our knowledge of the long-term sensitivity of the GrIS to climate changes.

2 Study site and previous work

Inglefield Land is situated in north Greenland, between 78.2–79.1° N and 65.8–72.8° W, and is bound to the south and east by the GrIS, to the west by Smith Sound, and to the north by Kane Basin and Humboldt Glacier (Fig. 1). Humboldt Glacier drains ca. 5 % of the GrIS into Nares Strait and has a varied velocity profile due to diverse bed topography and drainage networks (Rignot and Kanagaratnam, 2006; Hill et al., 2017; Livingstone et al., 2017). In addition to the marine terminating Humboldt Glacier, the land-based Hiawatha Glacier is present in the eastern part of Inglefield Land. Together with the GrIS, this glacier overlies the newly discovered Hiawatha impact crater, which makes the ice form a half circular structure, characterized by ice that flows faster than the rest of the ice margin terminating on land in Inglefield Land (Kjær et al., 2018).

The region is a high-Arctic desert, with low precipitation rates of ca. 100–150 mm yr^{-1}, falling mostly as snow (Blake et al., 1992; Dawes, 2004). The bedrock in the area is composed of Paleoproterozoic granite and gneiss, Late Proterozoic sedimentary and volcanic rocks, and Lower Paleozoic sedimentary rocks and shelf carbonates with Quaternary deposits close to the present-day ice margin (Dawes, 2004; Kolb et al., 2016). The relief is gently declining from 600 to 700 m a.s.l. close to the present-day ice margin towards the coast where meltwater channels and rivers cut the up to ca. 400 m high plateaus composed of sedimentary rocks (Dawes, 2004).

During the Last Glacial Maximum (LGM) the GrIS and Inuitian Ice Sheet coalesced in Nares Strait and the ice flowed north- and southward from a saddle in Kane Basin (England et al., 2006). The southward flowing ice formed the Smith Sound Ice Stream (England et al., 2006; Jennings et al., 2019), and it is believed to have extended to the 600 m depth contour in northern Baffin Bay (Funder et al., 2011). Radiocarbon ages reveal that deglaciation of Nares Strait was initiated at the northern entrance ca. 11 ka cal BP and southern entrance ca. 10 ka cal BP (Bennike and Björck, 2002; Jennings et al., 2011). The final deglaciation and opening of Nares Strait have been debated but recent off-shore studies together with a few terrestrial studies place the collapse of the ice saddle in Kane Basin and opening of Nares Strait between ca. 9–8 ka cal BP (Georgiadis et al., 2018; Jennings et al., 2019; Dalton et al., 2020). Recently, Jakobsen et al. (2018) and Reusche et al. (2018) proposed an overall glacial retreat of the GrIS in north Greenland during the Holocene, but with a possible stillstand of the ice sheet and its outlet glaciers as a response to the 8.2 ka cold events. These studies further suggested a restricted extent of the ice sheet in the Middle and Late Holocene, until ca. 0.3 ka where the ice reached its Little Ice Age (LIA) position.

The glacial history of Inglefield Land comprises the history of the Smith Sound Ice Stream along the coast and the history of the GrIS in Inglefield Land, as described by Nichols (1969), Tedrow (1970) and Blake et al. (1992), with additional evidence from the neighbouring Humboldt Glacier and Washington Land to the east by Bennike (2002) and Reusche et al. (2018). The deglaciation of the interior parts of Inglefield Land is less well known but a set of distinct moraine systems between the present-day ice margin and the

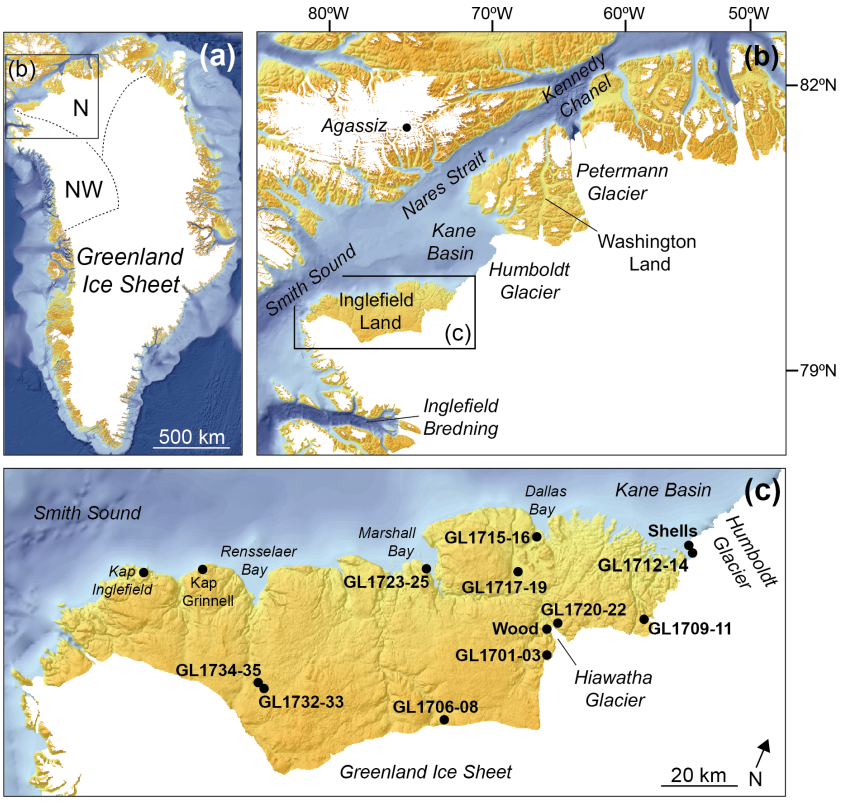

Figure 1. Location of the study area in Greenland **(a)**, with marked northwest (NW) and north (N) Greenland extent and places mentioned in the text **(b)**. Panel **(c)** shows Inglefield Land with places discussed in the text. Black dots denote sample locations for wood fragments in front of the Hiawatha Glacier, molluscs at the margin of the Humboldt Glacier and boulder samples (GL17XX) collected throughout the study area.

coastline (Nichols, 1969) suggest that the GrIS made several stops or re-advances during the overall deglaciation of Inglefield Land. Our current knowledge about the timing of deglaciation in Inglefield Land comprises a number of minimum limiting radiocarbon ages of raised marine deposits from the coastal areas that range from ca. 8.6 to 6.6 ka cal BP (Nichols, 1969; Blake et al., 1992; Mason, 2010). The marine limit in Inglefield Land has been determined at several locations and decreases from ca. 90 m in the southwestern part of Inglefield Land to ca. 65 m in the northeastern part of Inglefield Land (Nichols, 1969; Funder and Hansen, 1996).

3 Methods

3.1 Cosmogenic nuclide exposure dating

Cosmogenic nuclide exposure dating is a widely used method to constrain the deglaciation history of former glaciated areas (Gosse and Phillips, 2001; Ivy-Ochs and Kober, 2008; Balco, 2020). One of the most common nuclides used is ^{10}Be as it forms in the abundant mineral quartz, and is fairly easy to extract and measure by accelerator mass spectrometry. However, due to its relatively slow decay and long half-life (1.4×10^6 years), problems can arise in areas characterized by slow-moving cold-based ice. Here, small rates of erosion hinder complete removal of nuclides "inherited" from prior exposures and thus yield apparent exposure ages exceeding the length of the last ice-free period (Heyman et al., 2011). Nuclide inheritance is present in samples throughout Greenland, particularly at high elevations away from glacial troughs and fjords (Kelly et al., 2008; Corbett et al., 2013; Håkansson et al., 2016; Young et al., 2020), but it seems to be especially frequent in north Greenland where several studies have shown more widespread nuclide inheritance (Farnsworth et al., 2018; Larsen et al., 2018, 2020; Søndergaard et al., 2019; Ceperley et al., 2020).

Measurements of in situ produced ^{14}C in boulders and bedrock can, however, circumvent the nuclide inheritance problem and help to obtain more reliable exposure ages (Hippe, 2017; Graham et al., 2019). Due to its shorter half-life (5730 years), in situ ^{14}C is sensitive to radioactive decay on Late Quaternary and Holocene timescales, as the concentration build-up from prior exposure will rapidly decay when a surface is shielded from cosmic rays (Lifton et al., 2001; Hippe, 2017). As such, it is an optimal tool to solve the most recent deglaciation history of the GrIS. However, in situ ^{14}C is still not the preferred nuclide for exposure dating as the

extraction process is demanding despite many improvements and developments within recent years (Lifton et al., 2015; Goehring et al., 2019; Lupker et al., 2019). Still more robust information on the deglaciation history can be achieved by using combined measurements of ^{10}Be and ^{14}C as shown by previous studies (Corbett et al., 2013; Hippe, 2017; Young et al., 2018; Graham et al., 2019).

3.1.1 ^{10}Be exposure dating

^{10}Be exposure dating of boulders and pebbles was used to constrain the most recent deglaciation history of Inglefield Land. A total of 25 boulder samples were collected, all resting on bedrock except for sample GL1732-GL1735, which were on top of two moraines in the western part of Inglefield Land (Fig. 1c). The lithology of boulders sampled were all granite or gneiss, matching the lithology in and around Inglefield Land, but due to the placement on bedrock and moraines we assume the boulders were transported some distance before deposition. In addition, two samples consisting of quartz pebbles (GL1715 and GL1716) were collected on an outwash plain in the northeastern part of Inglefield Land. Samples were collected using a rock saw, hammer and chisel to cut out the top few centimetres of quartz bearing stable boulders (Fig. 2). With a hand-held Garmin eTrex 30 GPS, we recorded the latitude, longitude and elevation of each sample. The orientation of the rock surface and shielding by the surrounding topography were measured using a compass and clinometer, respectively. Elevations of the sampled boulders were all between 65 and 542 m a.s.l. and thus were all at or above the local marine limit of the area (Nichols, 1969; Blake et al., 1992; Funder and Hansen, 1996). We measured sample thicknesses with a caliper before the samples were crushed and sieved. This information was used to calculate the average thickness of each sample. For boulder and pebble samples we used the 250–700 µm fraction to isolate quartz and extract beryllium.

All samples were processed in the Cosmogenic Nuclide Laboratory at the Department of Geoscience, Aarhus University following methods adapted from Corbett et al. (2016). The ^{10}Be/^{9}Be ratios were measured at the Aarhus AMS Centre and all samples were blank corrected. Nuclide concentrations were normalized to the Beryllium Standard ICN-01-5-4, with a ^{10}Be/^{9}Be value of 2.851×10^{-12} (Nishiizumi et al., 2007). Apparent ^{10}Be exposure ages were calculated using the online exposure age calculator formerly known as the CRONUS-Earth online exposure calculator v.3 (Balco et al., 2008) in combination with the Baffin Bay production rate (Young et al., 2013) and the Lm production scaling scheme (Lal, 1991; Stone, 2000). The rock density was set to 2.65 g m^{-3} as it is representative for the boulders we sampled, and we assumed zero erosion. We did not correct for cover by vegetation or snow as the vegetation in the area is sparse and precipitation rates are low, ca. 100–150 mm yr^{-1} (Dawes, 2004). The sampled boulders were furthermore all positioned in open locations in the landscape making it highly unlikely that any snow cover would have persisted for long periods of time. As the glaciostatic uplift history is not well constrained in north Greenland, we present our ^{10}Be ages without any uplift correction, similarly to many other studies in Greenland which have shown the corrections to be negligible (Young et al., 2012; Sinclair et al., 2016; Larsen et al., 2018; Young et al., 2020).

All resulting apparent exposure ages and parameters used in the calculations can be seen in Table 1. The ^{10}Be ages are presented with a 1σ analytical uncertainty, and we note that ages calculated using other scaling schemes deviate by < 2 %.

3.1.2 In situ ^{14}C exposure dating

We used in situ ^{14}C exposure dating to further constrain the deglaciation history of Inglefield Land, primarily by testing for ^{10}Be nuclide inheritance in selected samples. Four of the quartz samples used for ^{10}Be exposure dating were chosen for in situ ^{14}C exposure dating, GL1725, GL1712, GL1701 and GL1708. We chose these samples based on (i) the resulting apparent ^{10}Be exposure ages within each sample location, (ii) the amount of quartz left and (iii) the sample location in the study area to secure a broad spatial distribution (Fig. 1c). Approximately 4 g of purified quartz, the same used for ^{10}Be extraction, was used to extract the in situ produced ^{14}C. Samples for in situ ^{14}C measurements were processed using the in situ ^{14}C extraction line at ETH Zürich (Hippe et al., 2009; Lupker et al., 2019). Samples were measured at ETH Zürich with the MICASAS AMS system (Synal et al., 2007; Wacker et al., 2010) and sample in situ ^{14}C concentrations were calculated from measured ^{14}C/^{12}C ratios (Hippe and Lifton, 2016). In situ ^{14}C ages were calculated using the online exposure age calculator formerly known as the CRONUS-Earth online exposure calculator v.3 (Balco et al., 2008), the west Greenland production rate (Young et al., 2014) and the Lm production scaling scheme (Lal, 1991, Stone, 2000). All resulting ages and variables used in the calculations are listed in Table 2. In situ ^{14}C exposure ages are presented with a 1σ analytical uncertainty and ages calculated using other scaling schemes deviate by < 4 %.

3.2 Radiocarbon dating of reworked molluscs and wood fragments

Radiocarbon dating of reworked organic material in glacial deposits can be used to determine when the ice extent was smaller than it is at present (Bennike and Weidick, 2001; Briner et al., 2014; Farnsworth et al., 2018). For this purpose, we therefore collected reworked marine molluscs from the surface of and within diamictic sediments at the southern margin of the Humboldt Glacier (Fig. 1c). From the sample site, 15 molluscs were chosen, pre-treated following the procedure of Brock et al. (2010), and radiocarbon dated at the

Table 1. Sample collection, ^{10}Be isotopic information and resulting exposure ages for 25 boulder and 2 pebble samples from Inglefield Land, north Greenland.

Sample name	Sample type	Elevation (m a.s.l.)	Latitude (° N)	Longitude (° W)	Sample thickness (cm)	Shielding correction	Quartz (g)	Carrier added (g)[a]	Sample ^{10}Be/^{9}Be ratio (10^{-14})	Blank ^{10}Be/^{9}Be ratio (10^{-14})	^{10}Be conc. (atoms g^{-1})	^{10}Be unc. (atoms g^{-1})	^{10}Be age (ka)[b]
GL1701	Boulder	542	78.76	−67.01	5.8	0.9999	40.006	0.739	130.9 ± 2.8	0.3 ± 0.08	529 068	13 417	76.9 ± 2.0
GL1702	Boulder	533	78.76	−67.01	5.2	0.9997	40.046	0.751	30.0 ± 5.7	0.3 ± 0.08	122 306	23 513	17.6 ± 3.4
GL1703	Boulder	530	78.76	−67.02	5.7	0.9994	40.084	0.762	75.4 ± 1.1	0.3 ± 0.08	312 981	6183	45.7 ± 0.9
GL1706	Boulder	521	78.51	−67.94	5.3	0.9997	40.176	0.751	45.3 ± 1.0	0.3 ± 0.08	184 398	4623	26.9 ± 0.7
GL1707	Boulder	524	78.51	−67.94	5.7	0.9997	40.428	0.756	57.0 ± 0.9	0.3 ± 0.08	232 494	4811	34.0 ± 0.7
GL1708	Boulder	524	78.51	−67.94	5.4	0.9998	40.071	0.752	55.0 ± 1.0	0.3 ± 0.08	225 228	5069	32.8 ± 0.7
GL1709	Boulder	159	78.94	−67.02	5.4	0.9952	40.043	0.602	17.2 ± 0.8	0.3 ± 0.08	55 336	2595	11.8 ± 0.6
GL1710	Boulder	159	78.94	−67.02	5.3	0.9963	40.050	0.603	13.7 ± 1.1	0.3 ± 0.08	43 909	3758	9.3 ± 0.8
GL1711	Boulder	163	78.94	−66.02	4.8	0.9950	40.065	0.205	47.6 ± 2.5	0.02 ± 0.01	154 443	8090	32.7 ± 1.7
GL1712	Boulder	65	79.14	−65.81	5.6	0.9998	34.035	0.206	11.9 ± 0.9	0.02 ± 0.01	45 662	3555	10.8 ± 0.8
GL1713	Boulder	67	79.14	−65.81	5.3	0.9998	40.261	0.214	10.5 ± 0.7	0.02 ± 0.01	35 421	2451	8.3 ± 0.6
GL1714	Boulder	67	79.14	−65.81	6.0	0.9999	40.088	0.214	11.3 ± 1.4	0.02 ± 0.01	38 144	4846	9.0 ± 1.1
GL1715	Pebbles	58	79.03	−67.80	0.7	0.9999	40.235	0.205	9.2 ± 2.6	0.02 ± 0.01	29 660	8520	6.8 ± 2.0
GL1716	Pebbles	58	79.03	−67.80	2.2	0.9999	40.196	0.212	20.9 ± 5.6	0.02 ± 0.01	69 622	18 782	16.2 ± 4.4
GL1717	Boulder	195	78.93	−67.82	6.0	0.9981	40.114	0.443	9.8 ± 0.5	0.02 ± 0.01	68 250	3283	14.0 ± 0.7
GL1718	Boulder	195	78.93	−67.82	5.7	0.9981	40.012	0.210	64.8 ± 10.5	0.02 ± 0.01	215 174	34 752	44.4 ± 7.3
GL1719	Boulder	191	78.93	−67.82	3.9	0.9997	40.031	0.207	19.7 ± 0.8	0.02 ± 0.01	64 477	2743	13.0 ± 0.5
GL1720	Boulder	284	78.84	−67.09	3.3	0.9993	40.159	0.215	23.3 ± 0.9	0.02 ± 0.01	78 937	3097	14.3 ± 0.6
GL1721	Boulder	302	78.84	−67.09	3.9	0.9983	40.038	0.208	28.9 ± 0.7	0.2 ± 0.05	94 273	2377	17.0 ± 0.4
GL1722	Boulder	301	78.84	−67.09	4.5	0.9983	40.016	0.205	30.3 ± 0.7	0.2 ± 0.05	99 077	2296	17.9 ± 0.4
GL1723	Boulder	87	78.85	−68.89	4.7	0.9989	40.039	0.203	12.8 ± 0.5	0.2 ± 0.05	40 899	1501	9.4 ± 0.3
GL1724	Boulder	82	78.85	−68.89	5.6	0.9992	40.024	0.206	12.3 ± 0.4	0.2 ± 0.05	39 377	1370	9.1 ± 0.3
GL1725	Boulder	86	78.85	−68.89	5.7	0.9991	40.006	0.203	53.8 ± 0.9	0.2 ± 0.05	172 559	3088	40.2 ± 0.7
GL1732	Boulder	483	78.41	−70.32	4.6	1	40.059	0.201	124.6 ± 1.5	0.2 ± 0.05	396 868	5565	60.2 ± 0.9
GL1733	Boulder	483	78.41	−70.32	5.6	1	39.648	0.201	168.7 ± 1.9	0.2 ± 0.05	542 019	7114	83.4 ± 1.1
GL1734	Boulder	480	78.41	−70.33	4.9	1	34.450	0.204	158.9 ± 2.2	0.2 ± 0.05	602 773	9256	92.7 ± 1.5
GL1735	Boulder	482	78.41	−70.33	5.3	1	40.007	0.208	147.0 ± 1.5	0.2 ± 0.05	484 687	5982	74.3 ± 0.9

[a] Carrier *Phe1602* (328.2 ± 3.7 µg ^{9}Be g^{-1}) was used for preparation of sample GL1701–GL1703 and GL1706–GL1710. All other samples were prepared using carrier *Phe1603* (949.4 ± 6.2 µg ^{9}Be g^{-1}). [b] ^{10}Be ages were calculated using the online exposure age calculator formerly known as the CRONUS-Earth online exposure calculator v.3 (Balco et al., 2008), the Baffin Bay production rate (Young et al., 2013) and the St scaling scheme (Lal, 1991; Stone, 2000) under standard atmosphere conditions. A rock density of 2.65 g cm^{-3} was used and we assumed zero erosion. Samples were normalized to the Beryllium Standard ICN-01-5-4, with a ^{10}Be/^{9}Be value of 2.851 $\times 10^{-12}$ (Nishiizumi et al., 2007), and blank corrected. ^{10}Be age uncertainties are reported as the 1σ internal uncertainty.

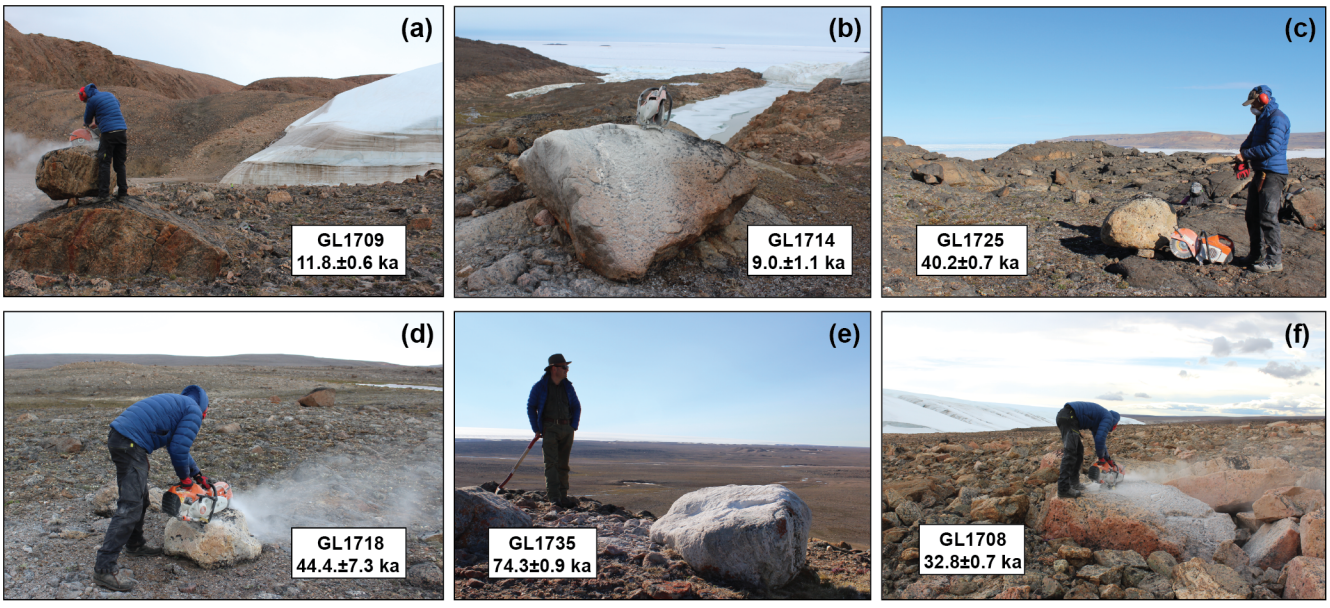

Figure 2. Boulders sampled for ^{10}Be exposure dating in Inglefield Land **(a–f)**, as well as resulting ages. Panels **(a)** and **(f)** show boulders sampled close to the present-day ice margin. Panel **(b)** is a boulder sampled next to the Humboldt Glacier. Panels **(c)** and **(d)** show boulder samples close to the outer coast. Panel **(e)** shows a boulder sampled on a moraine in the western part of the study area.

Table 2. Sample collection, ^{14}C isotopic information and resulting exposure ages for four boulders from Inglefield Land, north Greenland.

Sample name	Elevation (m a.s.l.)	Latitude (° N)	Longitude (° W)	Shielding correction	Quartz (g)	CO_2 yield (µg)	$F^{14}C^{a}$	$\delta^{13}C$ (‰)	$^{14}C/^{12}C_{total}$ (10^{-14})	^{14}C atoms blank corrected (10^5)^{b}	^{14}C (10^5 at g^{-1})	^{14}C exposure age (ka)^{c}
GL1701	542	78.76	67.01	0.9999	3.9552	22.93	0.550	−10.1	65.0 ± 0.71	6.88 ± 0.10	1.74 ± 0.03	14.2 ± 0.5
GL1708	524	78.51	67.94	0.9998	3.9036	76.28	0.114	−10.8	13.4 ± 0.25	4.54 ± 0.11	1.16 ± 0.03	6.7 ± 0.3
GL1712	65	79.14	65.81	0.9998	3.9156	80.01	0.083	−12.9	9.70 ± 0.23	3.30 ± 0.11	0.84 ± 0.03	8.2 ± 0.5
GL1725	86	78.85	68.89	0.9991	3.8113	77.42	0.083	−11.6	9.77 ± 0.23	3.20 ± 0.10	0.84 ± 0.03	7.9 ± 0.4

[a] Normalized to $\delta^{13}C$ of −25 ‰ VPDB and AD 1950. [b] All samples were blank corrected (0.589 ± 0.052 10^5 ^{14}C atoms). [c] 14C ages were calculated using the online exposure age calculator formerly known as the CRONUS-Earth online exposure calculator v.3 (Balco et al., 2008), the west Greenland production rate (Young et al., 2014) and the Lm scaling scheme (Lal, 1991; Stone, 2000) under standard atmosphere conditions. A rock density of 2.65 g cm^{-3} was used and we assumed zero erosion. ^{14}C age uncertainties are reported as the 1σ analytical uncertainty.

Aarhus AMS Centre (Olsen et al., 2016). In addition, four wood fragments were retrieved at 193 m a.s.l. on the meltwater plain next to the meltwater outlet at the Hiawatha Glacier (Fig. 1c). Due to the placement of the wood fragments at the tip of the glacier, we assume the wood was transported from underneath the glacier a distance up the ice, before deposition at the glacier front. The wood fragments were collected together with sediment samples analysed in recent studies concerning the Hiawatha impact crater (Kjær et al., 2018; Garde et al., 2020). It was not possible to identify the dated wood fragments to species level. The four samples were pre-treated and radiocarbon dated at Beta Analytic.

Radiocarbon ages for the molluscs were calibrated using OxCal v4.3 (Ramsey, 2009) with the Marine13 calibration curve (Reimer et al., 2013) and a marine reservoir effect of 550 ^{14}C years ($\Delta R = 150^{14}C$ a) based on a couple of ages from molluscs collected alive before 1960 in north Greenland (Mörner and Funder, 1990). Radiocarbon ages for the wood fragments were calibrated with the IntCal13 calibration curve (Reimer et al., 2013). Sample information, resulting radiocarbon ages and calibrated ages are reported in Table 3. Throughout the text, we use the mean calibrated radiocarbon age ±2σ.

4 Results

4.1 ^{10}Be and in situ ^{14}C exposure dating

^{10}Be exposure dating was carried out on 25 boulder samples and 2 samples consisting of pebbles to constrain the deglaciation of Inglefield Land (Fig. 3). The measured ^{10}Be concentrations in the 27 samples range from $3.0 \pm 0.9 \times 10^4$ to $60.3 \pm 0.9 \times 10^4$ ^{10}Be atoms g^{-1} and result in apparent exposure ages ranging from 92.7 ± 1.5 to 6.8 ± 2.0 ka, with the oldest ages being from boulders on moraines in the western

Table 3. Sample collection information, radiocarbon ages and calibrated ages for marine molluscs collected at the margin of the Humboldt Glacier and wood fragments collected in front of the Hiawatha Glacier, north Greenland.

Lab ID	Sample material	Latitude (° N)	Longitude (° W)	Elevation (m a.s.l.)	Age (^{14}C years BP)	Age (95 % range) (cal. years BP)*	Mean age (cal. years BP $\pm 2\,\sigma$)*
AAR-27511	*Mya truncata*				2006 ± 24	1321–1494	1400 ± 44
AAR-27512	*Mya truncata*				1589 ± 22	920–1050	983 ± 35
AAR-27513	*Mya truncata*				3387 ± 34	2937–3166	3052 ± 60
AAR-27514	*Mya truncata*				2899 ± 27	2345–2606	2466 ± 70
AAR-27515	*Mya truncata*				3831 ± 26	3501–3684	3593 ± 44
AAR-27516	*Mya truncata*				1093 ± 20	499–605	542 ± 28
AAR-27517	*Mya truncata*				1415 ± 23	736–891	812 ± 41
AAR-27518	*Hiatella arctica*	79.143	65.797	90	3413 ± 25	2984–3181	3087 ± 50
AAR-27519	*Hiatella arctica*				1988 ± 28	1299–1474	1379 ± 45
AAR-27520	*Hiatella arctica*				1195 ± 23	553–662	613 ± 30
AAR-27521	*Hiatella arctica*				2580 ± 25	1979–2148	2066 ± 45
AAR-27522	*Hiatella arctica*				1428 ± 23	749–900	825 ± 39
AAR-27523	*Hiatella arctica*				2318 ± 33	1698–1884	1793 ± 49
AAR-27524	*Hiatella arctica*				2248 ± 22	1666–1865	1761 ± 49
AAR-27525	*Astarte borealis*				1466 ± 25	783–922	857 ± 38
471815	Wood				2260 ± 30	2158–2346	2256 ± 59
471816	Wood	78.830	67.133	193	1910 ± 30	1741–1929	1854 ± 37
471817	Wood				2260 ± 30	2158–2346	2256 ± 59
471818	Wood				5120 ± 30	5751–5930	5846 ± 59

* Radiocarbon ages were calibrated using OxCal v4.3 (Ramsey, 2009). The Marine13 calibration curve (Reimer et al., 2013) and a marine reservoir effect of 550 ^{14}C years ($\Delta R = 150$) (Mörner and Funder, 1990) were used for calibrating sample AAR-27511 to AAR-27525. For sample 471815–471818, the Intcall13 curve was used for calibration (Reimer et al., 2013).

part of the area and the younger ages resulting from boulders closer to Humboldt Glacier and the coast in the northeastern part of the area (Fig. 3, Table 1).

Although the ^{10}Be ages are scattered we see some structure in the dataset. There is no clear pattern between the lithology of the individual boulders sampled and the resulting exposure ages, but the majority of ages sampled below 300 m a.s.l. group within the post-LGM period, with a peak in the Early Holocene, whereas most samples above 450 m a.s.l. predate the LGM. Further, there also seems to be a vague pattern in spatial distribution, with the oldest ^{10}Be ages being from the two moraine ridges in western Inglefield Land and the youngest boulder ages closer to Humboldt Glacier.

In situ ^{14}C exposure dating was carried out to better constrain the deglaciation of Inglefield Land from the scattered ^{10}Be ages. The measured in situ ^{14}C concentrations in the four samples range from $8.4 \pm 0.3 \times 10^4$ to $17.4 \pm 0.2 \times 10^4$ atoms g^{-1} and resulted in exposure ages ranging from 14.2 ± 0.5 to 6.7 ± 0.3 ka (Fig. 3, Table 2). All in situ ^{14}C ages are younger than the ^{10}Be ages resulting from the same quartz sample, confirming that the ^{10}Be ages are generally affected by nuclide inheritance. However, the in situ ^{14}C ages do to some degree match the youngest ^{10}Be ages from the same localities, except for GL1701, which predates the Holocene. The remaining three in situ ^{14}C ages group in the Middle Holocene.

4.2 Radiocarbon dating of reworked molluscs and wood fragments

Reworked marine molluscs were collected along the southern margin of the Humboldt Glacier (Fig. 1c). Several species were identified and 15 samples of *Mya truncata*, *Hiatella arctica* and *Astarte borealis* were used for radiocarbon dating. The calibrated mean radiocarbon ages range from 3.6 ± 0.04 to 0.5 ± 0.03 ka cal BP (Fig. 4, Table 3) and reflect the period when the Humboldt Glacier was behind its present-day extent. In addition, the wood samples on the meltwater plain next to the meltwater outlet at the Hiawatha Glacier resulted in ages between 5.8 ± 0.06 and 1.9 ± 0.04 ka cal BP (Fig. 4, Table 3). As the wood fragments were retrieved right in front of the Hiawatha Glacier, the wood fragments are more likely to have originated from underneath the glacier than have been transported from a nearby soil to the sample site by wind or water. We therefore believe these ages to constrain a time when the glacier was behind its present-day extent.

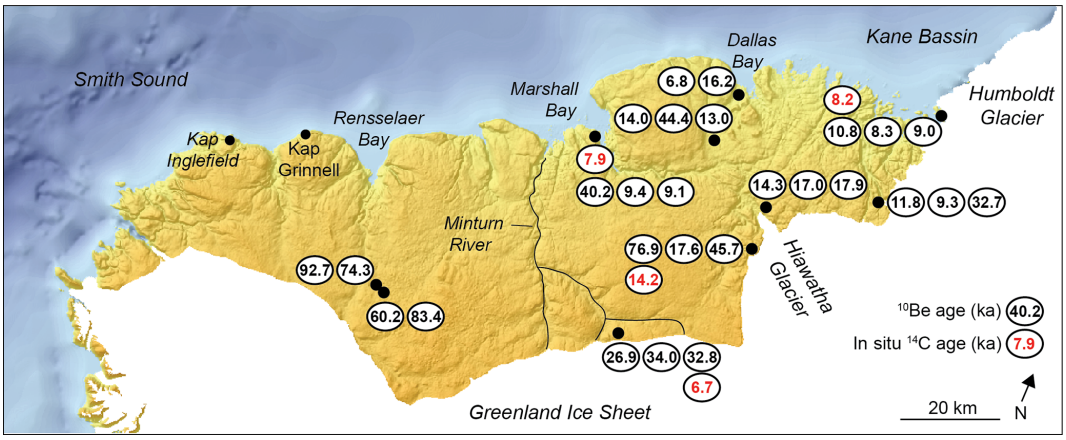

Figure 3. Map of Inglefield Land, north Greenland. Black dots denote sample locations for boulder samples and their resulting ^{10}Be and in situ ^{14}C exposure ages given in thousands of years (ka). ^{10}Be age uncertainties range between 0.3 and 7.3 ka with an average of 1.4 ka and ^{14}C age uncertainties range between 0.3 and 0.5 ka with an average of 0.4 ka.

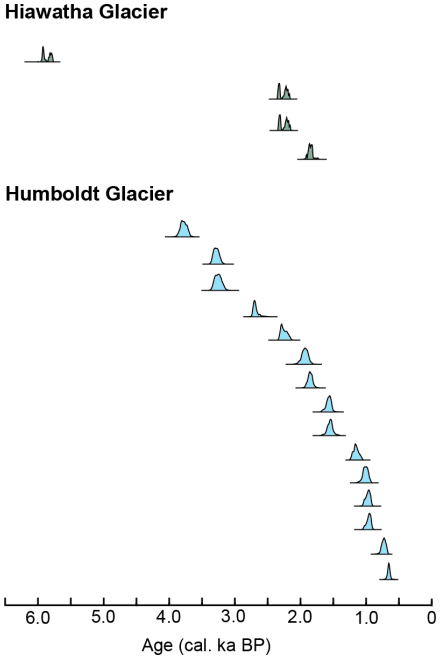

Figure 4. Radiocarbon age probability plots of wood fragments collected in front of the Hiawatha Glacier (green) and reworked marine molluscs collected at the margin of Humboldt Glacier (blue). Each plot represents the age of a single wood fragment or mollusc shell and its calibrated age probability distribution.

5 Discussion

5.1 Indications of low erosion rates and cold-based ice in north Greenland

The ^{10}Be ages from Inglefield Land are scattered, which makes it difficult to fully constrain the glacial history in the area. We consider the 12 ^{10}Be ages older than the LGM as evidence of nuclide inheritance from prior exposure (Fig. 3) and discard them from constraints of the glacial history in Inglefield Land. Of the remaining 15 samples postdating the LGM, some do most likely also reflect nuclide inheritance. Within uncertainty, only 4 of the 15 post-LGM ^{10}Be ages overlap with the 3 youngest in situ ^{14}C ages. Thus, by including in situ ^{14}C ages in the analysis we determine that 11 of the post-LGM ^{10}Be ages are affected by inheritance and thus overestimate the post-LGM exposure period to a varying degree. In total, 24 out of 27 samples (ca. 89 %) from Inglefield Land show some degree of nuclide inheritance.

We also consider the oldest in situ ^{14}C age of ca. 14.2 ka to be affected by inheritance as it is unlikely that Inglefield Land was deglaciated at that time. Different modelled scenarios of in situ ^{14}C nuclide build-up, which almost reach the measured concentration of the sample and still follow the known glacial history of the GrIS in north Greenland, are seen in Fig. 5. In the first scenario, Inglefield Land was deglaciated during MIS 3 from 45 to 23 ka and again in the Holocene from 6.7 ka until the present. This limits the expansion of the GrIS during the LGM to a narrow interval from ca. 23 to 7 ka. This scenario is to some degree consistent with other studies in northern Greenland where radiocarbon ages of marine molluscs show that the GrIS has had a restricted ice extent during MIS 3, starting as early as ca. 42 ka cal BP (Larsen et al., 2018; Søndergaard et al., 2019), and a late coalescence of the GrIS and Inuitian Ice Sheet around 22 ka cal BP (England, 1999). We have tried different model runs, including letting the initial concentration be at saturation (starting the model at 60 ka), but due to the short half-life of ^{14}C, any concentration build-up prior to our constrained period only results in a very small increase in the final present-day concentration (ca. 5 %). Therefore exposure prior to 45 ka is not the main reason for the remaining "inheritance".

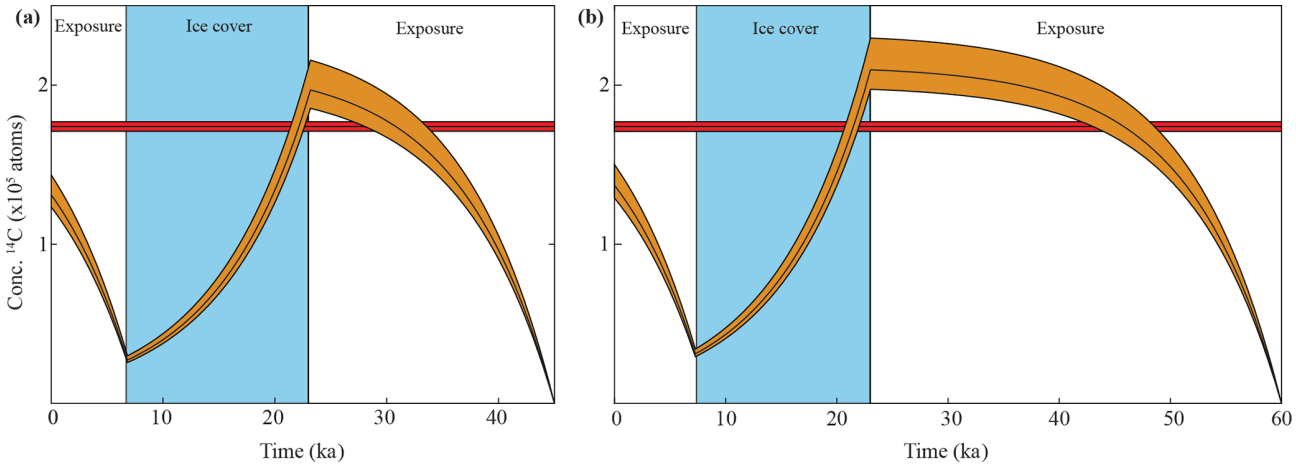

Figure 5. Modelled exposure scenario for boulder sample GL1701. The red line shows the measured in situ ^{14}C concentration in the sample and the orange line is the nuclide concentration build-up and decay during periods of exposure and ice cover. Panel **(a)** shows exposure from 45 to 23 ka and again from 6.7 ka until present and ice cover in between. Panel **(b)** shows exposure from 60 to 23 ka and again from 6.7 ka until present and ice cover in between.

However, as we only have one data point and the simulation is incapable of fully reaching the measured concentration we cannot make any firm conclusions on the timing of prior exposure of the sample and its implication for the ice sheet history.

The trend between apparent ^{10}Be ages and elevation of the samples point towards larger amount of inheritance in samples from higher elevations (Fig. 6). This pattern has also recently been observed in adjacent Washington Land as well as in Dove Bugt, northeast Greenland (Ceperley et al., 2020; Skov et al., 2020). In addition, there is an increasing amount of inheritance in samples farther away from the Humboldt Glacier. This spatial distribution of samples with inheritance at higher elevations away from the Humboldt Glacier is expected as these locations represent areas outside troughs where erosion is low because of slowly moving or even cold-based ice. A similar relationship between nuclide inheritance and elevation and distance to deep fjords with large fast-flowing outlet glaciers indicative of higher erosion rates has been demonstrated elsewhere in Greenland (Larsen et al., 2014; Søndergaard et al., 2019).

Overall, inheritance and the lack of sufficient nuclide resetting are widespread problems, especially in north Greenland, and have complicated several studies within recent years (Corbett et al., 2015; Farnsworth et al., 2018; Søndergaard et al., 2019; Ceperley et al., 2020; Larsen et al., 2020). Thus, we conclude that large parts of the north GrIS were inefficient at eroding the subglacial topography during parts of or throughout the last glaciation. This is probably because subglacial sliding was limited by cold-based thermal conditions and the overall low ice flux resulting from the relatively small precipitation rates of the region. We note that cold-based zones are also considered to dominate the present-day thermal state of the GrIS (MacGregor et al., 2016).

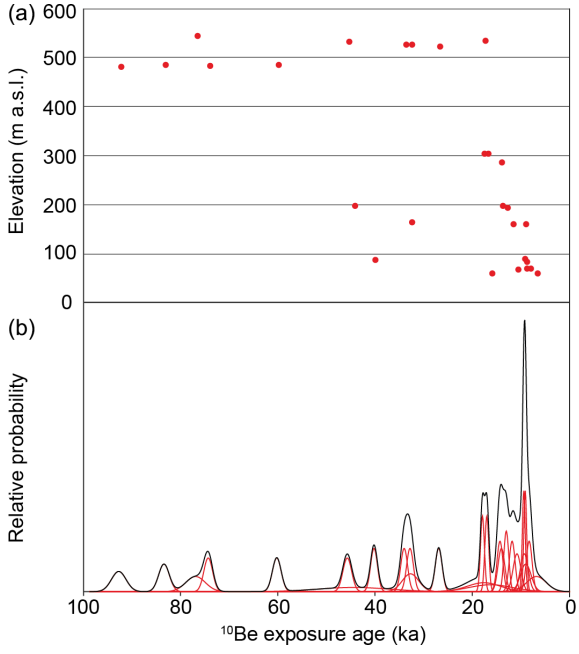

Figure 6. ^{10}Be ages from boulders sampled at various elevations in Inglefield Land, north Greenland. Panel **(a)** shows ^{10}Be ages plotted against elevation of the sample sites. Each red dot represents the ^{10}Be age of an individual boulder and its associated elevation. Panel **(b)** shows the relative probability distribution of the boulder ages with their 1σ analytical uncertainty (red lines) and the cumulated probability plot of all ^{10}Be ages (black line).

5.2 Holocene glacial history of Inglefield Land

During the LGM, Inglefield Land was completely ice covered, and the ice nourished the Smith Sound Ice Stream primarily through the Humboldt Glacier until the opening of

Nares Strait sometime between ca. 9 and 8 ka cal BP (Georgiadis et al., 2018; Jennings et al., 2019; Dalton et al., 2020). The outer coast at Kap Inglefield, Kap Grinnel and Rensselaer Bay in southwest Inglefield Land was deglaciated between ca. 8.6 and 8.3 ka cal BP (Nichols, 1969; Blake et al., 1992; Mason, 2010). Farther north, the deglaciation at the outer coast at Marshall Bay in central Inglefield Land is constrained to ca. 7.9 ka by a single in situ ^{14}C age. This age is largely consistent with a radiocarbon age of marine molluscs of ca. 8.2 ka cal BP at Minturn Elv located ca. 20 km east of Marshall Bay (Nichols, 1969) (Fig. 7a).

After reaching the outer coast, the ice margin continued its retreat towards its present-day position, which was reached by ca. 6.7 ka in the central part of Inglefield Land. Farther north, the ice probably retreated somewhat slower as suggested by the dating of a rearrangement of the meltwater drainage pattern from the Hiawatha Glacier. Initially, meltwater flowed from the Hiawatha Glacier towards Dallas Bay, but this changed when the ice margin was approximately halfway between the coast and its present-day extent where a water divide then rerouted the meltwater towards Marshall Bay (Nichols, 1969). The timing of this change is constrained by a single ^{10}Be age of meltwater deposits (pebble sample) that yield an age of ca. 6.8 ka (Fig. 7b). The ^{10}Be age is, however, consistent with a radiocarbon age of molluscs, presumably from lower-lying prodeltaic sediments, with an age of ca. 6.6 ka cal BP at Dallas Bay (Nichols, 1969). This suggests that the ice margin was located north of the meltwater drainage divide around ca. 6.8 ka. Farthest north in Inglefield Land, at the southern flank of the Humboldt Glacier, the ice margin already reached its present-day extent by ca. 8.2 ka (Fig. 7a). This age is consistent with the ^{10}Be chronology from the northern flank of the Humboldt Glacier where a moraine a few hundred metres outside the LIA moraine was abandoned at ca. 8.3 ka (Reusche et al., 2018).

After the ice margin reached its present-day position it continued to retreat farther inland. Wood fragments in front of the Hiawatha Glacier demonstrate that the land-based part of the GrIS in Inglefield Land was smaller than present between ca. 5.8 and 1.9 ka cal BP. In addition, the age distribution of the molluscs collected at the Humboldt Glacier margin indicates that the glacier was behind its present-day position between ca. 3.6 to 0.5 ka cal BP (Fig. 7a). At the northern flank of Humboldt Glacier, radiocarbon ages of reworked marine molluscs suggest that the glacier retreated at least 25 km farther inland between ca. 3.7 and 0.3 ka cal BP (Bennike, 2002), possibly favoured by the bed topography being below sea level tens of kilometres inland (Morlighem et al., 2014, 2017). Thus, no later than ca. 0.3 ka cal BP, the GrIS in Inglefield Land re-advanced towards its LIA maximum extent. The spatial extent of the Late Holocene retreat of the Hiawatha Glacier behind its present-day ice margin is not known, but the ice retreat has possibly exposed parts of the Hiawatha impact crater (Fig. 7b).

5.3 A review of the Holocene glacial history in northwest and north Greenland

In the following we review the new data from northwest and north Greenland to put our results into a broader context. We focus on two stages of the deglaciation history of the GrIS, namely when it (i) deglaciated from the coast towards its present-day extent and (ii) when it was smaller than present (Fig. 8). For information about the offshore deglaciation history, the reader is referred to recent reviews by Georgiadis et al. (2018), Jennings et al. (2019) and Dalton et al. (2020).

In the southern part of northwest Greenland, the ice margin reached the outer coast near Upernavik at ca. 11.3 ka (Corbett et al., 2013) coinciding with the overall ice retreat in Melville Bay being initiated at ca. 11.6 ka (Søndergaard et al., 2020) (Fig. 8b). The ice reached the inner part of Upernavik Fjord at ca. 9.9 ka (Briner et al., 2013) and in Melville Bay the ice was already at its present-day extent at ca. 11.5 ka (Søndergaard et al., 2020) (Fig. 8b). Farther north, coastal deglaciation near Thule and Delta Sø began at ca. 10.8 ka (Corbett et al., 2015; Axford et al., 2019) and the ice margin reached its present-day extent at nearby Wax Lips Lake at ca. 10.1 ka (McFarlin et al., 2018). In Inglefield Bredning north of Thule the ice reached the inner parts of the fjord at ca. 11.9 ka (Søndergaard et al., 2019) (Fig. 8b). In north Greenland, results from Inglefield Land show that the deglaciation of the outer coast commenced at ca. 8.6 ka cal BP in the southeast and ca. 7.9 ka in the central part of the coastline, and the ice reached its present-day position in central Inglefield Land at ca. 6.7 ka. The Humboldt Glacier deglaciated and reached its present-day extent at ca. 8.2 ka. In the adjacent Washington Land, deglaciation of the outer coast is constrained to ca. 9.0 ka, with widespread deglaciation of the entire area evident at ca. 8.6 ka and absence of widespread glacial ice no later than 6.9 ka (Ceperley et al., 2020). Farther north, Petermann Glacier was positioned at the outer sill in Hall Basin ca. 8.7 (Jakobsson et al., 2018) and it reached its present-day position at ca. 6.9 ka (Reilly et al., 2019).

Restricted ice extent behind the present-day ice margin in northwest and north Greenland was widespread during large parts of the Middle and Late Holocene. At Upernavik and in Melville Bay, the ice sheet was behind its present-day position between ca. 9.1 and 0.4 ka cal BP (Bennike, 2008; Briner et al., 2013; Briner et al., 2014; Axford et al., 2019; Søndergaard et al., 2020) (Fig. 8c). Farther north, mosses from a local ice cap and subfossil plants from the GrIS show a smaller than present-day extent before ca. 3.3 ka cal BP around Qaanaaq and throughout most of the Holocene until ca. 1850 AD in the Thule area (Farnsworth et al., 2018; Axford et al., 2019; Søndergaard et al., 2019). In Inglefield Land, north Greenland, wood fragments in front of the Hiawatha Glacier suggest that the ice margin was behind its present-day extent from ca. 5.8 and 1.9 ka cal BP, whereas the Humboldt Glacier retreated at least 25 km inland at ca. 3.7 to 0.3 ka cal BP (Bennike, 2002). The Petermann Glacier

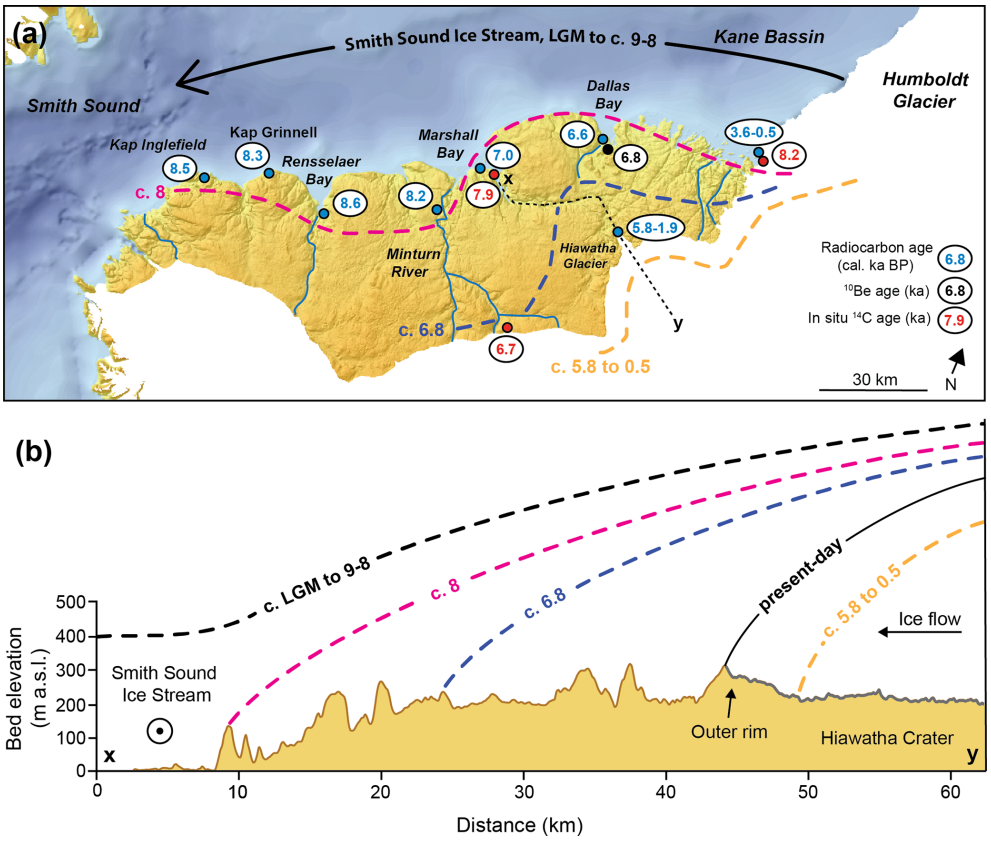

Figure 7. Deglaciation in Inglefield Land. Panel **(a)** shows ages believed to constrain the deglaciation in the area. In situ ^{14}C ages and radiocarbon ages at Humboldt Glacier and Hiawatha Glacier are from this study. Radiocarbon ages at the coast are from Nichols (1969), Blake et al. (1992) and Mason (2010). Panel **(b)** shows the Holocene deglaciation pattern in Inglefield Land inferred from this study across the transect (x–y) seen in panel **(a)**.

farther north also retreated inland from its present-day position and after a re-advance reached its LIA extent at ca. 0.3 ka (Reusche et al., 2018; Reilly et al., 2019) (Fig. 8c).

In summary, the timing of deglaciation along the coast in northwest Greenland is earlier than in north Greenland around Nares Strait, but the timing is in accordance with the overall deglaciation in Greenland (Bennike and Björck, 2002; Funder et al., 2011). Further, the periods of the Middle and Late Holocene restricted ice extent of the GrIS, and larger outlet glaciers in north Greenland were initiated later than in northwest Greenland and were shorter.

5.4 Holocene ice and climate interactions in northwest and north Greenland

The contrasting patterns of deglaciation between northwest and north Greenland can in part be explained by different responses of the two sectors to Holocene climate changes (Fig. 9). The early deglaciation of the land areas in northwest Greenland from Upernavik to Inglefield Bredning coincides with the early arrival of the Holocene Thermal Maximum (HTM) (ca. 11–8 ka) in northwest Greenland (Lecavalier et al., 2017; Axford et al., 2019) (Fig. 9a–c). This rapid increase in surface air temperatures has been suggested to be the main driver of the widespread rapid deglaciation specifically in Melville Bay, the Thule area and Inglefield Bredning (Axford et al., 2019; Søndergaard et al., 2019; Søndergaard et al., 2020), showing the sensitivity of marine-based ice to rising air temperatures.

In north Greenland, atmospheric temperatures during the Early and Middle Holocene were above those of the Late Holocene. The GrIS in this region could therefore have experienced a larger sensitivity towards atmospheric temperatures early in the Holocene. It has, however, been proposed that the effects of the retreating Innuitian Ice Sheet, which still covered Ellesmere Island during the Early Holocene, to some degree dampened the effect from the high atmospheric temperatures on the GrIS in western north Greenland during this period (Briner et al., 2016; Dalton et al., 2020). Further it has been suggested that warm Atlantic waters in Hall Basin, northern Nares Strait, assisted Early Holocene ice retreat (Jennings et al., 2011). Warm waters and increasing ocean temperatures in southern Nares Strait seemed to arrive later than along the west Greenland coast (Dyke et

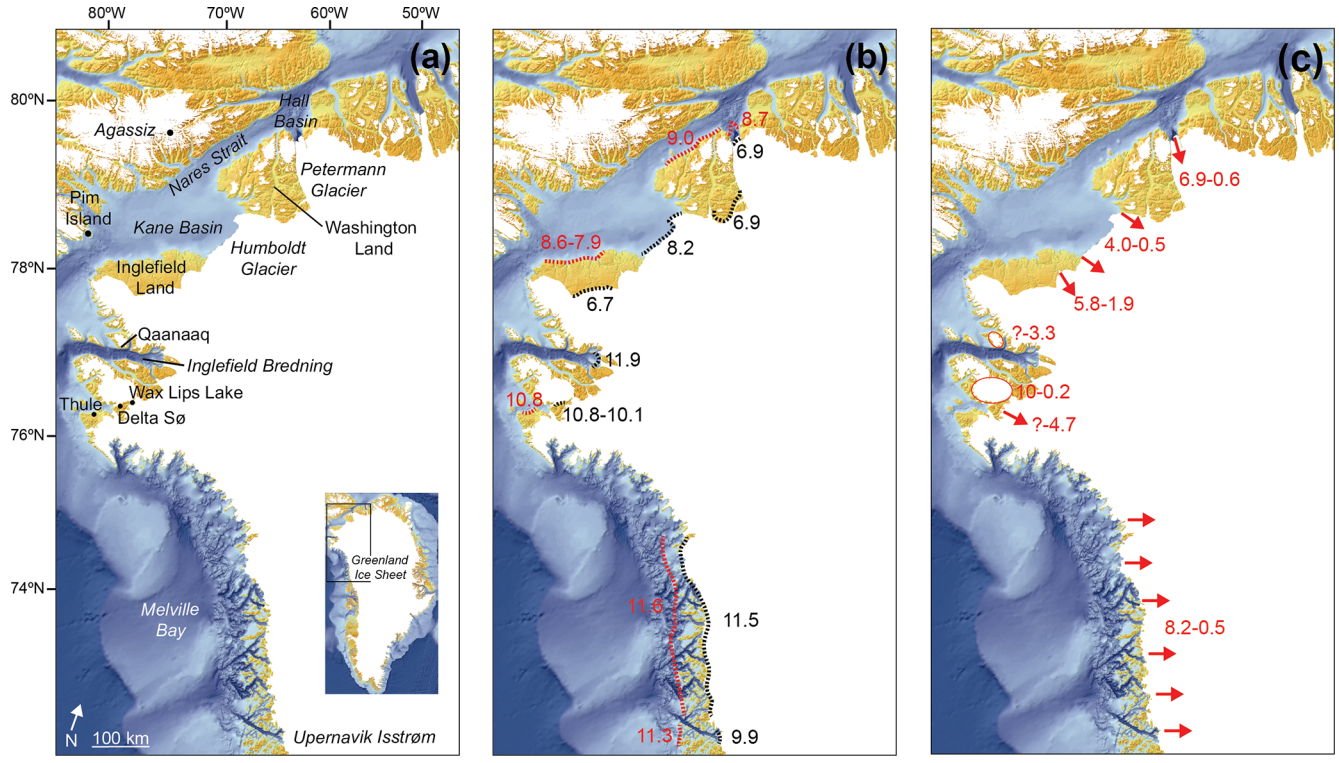

Figure 8. Age constraints (in ka) of the Holocene ice extent at the outer coast, present-day ice margin and for the period when the GrIS was smaller than present. Panel **(a)** shows localities in northwest and north Greenland. Panel **(b)** shows the initial Holocene deglaciation of the GrIS towards the outer coast (red) (Corbett et al., 2013, 2015; Jakobsson et al., 2018; Ceperley et al., 2020; Søndergaard et al., 2020) and following retreat towards the present-day ice margin (black) (Briner et al., 2013; McFarlin et al., 2018; Reusche et al., 2018; Axford et al., 2019; Reilly et al., 2019; Søndergaard et al., 2019; Ceperley et al., 2020; Søndergaard et al., 2020). Panel **(c)** shows the period when the GrIS and its outlets (arrows) and local ice caps (circles) were smaller than the present-day extent (Bennike, 2002, 2008; Briner et al., 2014; Farnsworth et al., 2018; Axford et al., 2019; Reilly et al., 2019; Søndergaard et al., 2019, 2020). A question mark means that the upper limit of restricted ice extent has not been constrained.

al., 1996; Levac et al., 2001; Lecavalier et al., 2017; Axford et al., 2019). This delay in warming ocean conditions in southern Nares Strait might be the reason why the opening of Nares Strait and the deglaciation of the coastal areas in Inglefield Land and Washington Land happened 2–3 kyr later than the land areas in northwest Greenland (Bennike and Björck, 2002; Larsen et al., 2014, 2019; Sinclair et al., 2016).

After the ice margin reached its present-day extent in northwest and north Greenland it continued to retreat farther inland. In northwest Greenland, the period with restricted ice extent in Melville Bay ca. 9.1 to 0.4 ka cal BP was driven by a strengthening of the West Greenland Current and warm ocean waters arriving in the Middle Holocene (Levac et al., 2001; Caron et al., 2020) (Fig. 9d). The presence of *Chlamys islandica* infers that the marine-based outlets were behind their present-day extent in north Greenland when warm waters arrived in Nares Strait (Bennike, 2002). Warming sea surface temperatures drove Middle Holocene ice sheet retreat, especially in northwest Greenland, but the overall retreat was possibly initiated and still affected by Early Holocene rising atmospheric temperatures.

The Neoglacial cooling is known to have affected ice on land in northwest Greenland, resulting in expansion of local ice caps, lake ice cover and even parts of the northwest GrIS (Blake et al., 1992; Lasher et al., 2017; Farnsworth et al., 2018; Søndergaard et al., 2019). The Hiawatha Glacier in north Greenland show a re-advance after ca. 1.9 ka cal BP, as a possible response to the Neoglacial cooling, which also seems to have provoked a re-advance of the Petermann Glacier at ca. 2.8 ka (Reusche et al., 2018). Finally, the ice in northwest and north Greenland shows a near-synchronous re-advance towards its LIA extent which coincides with the LIA cooling within the last millennium (Lasher et al., 2017; Lecavalier et al., 2017; Axford et al., 2019).

6 Conclusion

In this study we used in situ ^{10}Be and ^{14}C cosmogenic nuclide exposure dating and radiocarbon dating of reworked organic material to constrain the Holocene deglaciation history of Inglefield Land, north Greenland. Our results revealed a large scatter in the ^{10}Be ages, with ca. 45 % of the ages pre-

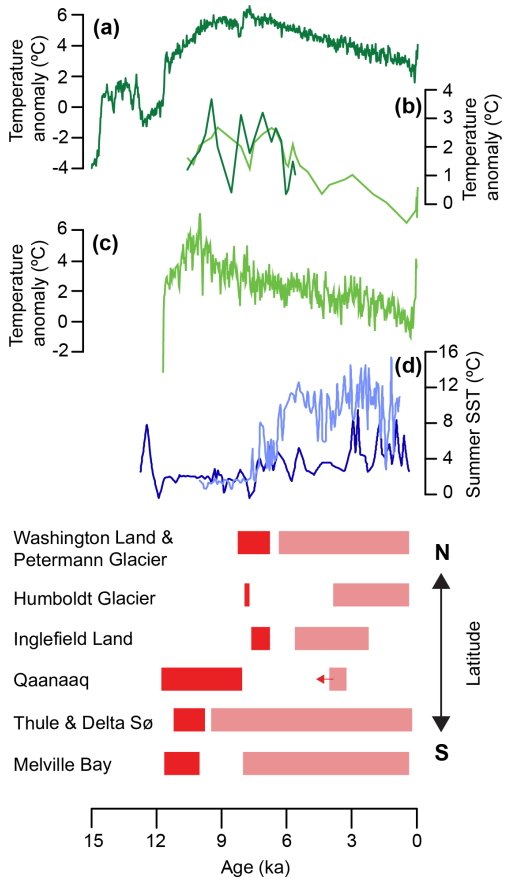

Figure 9. Ice extent and climate fluctuations for north and northwest Greenland during the last 15 kyr. **(a)** Mean annual temperature anomalies, northwest Greenland (Buizert et al., 2018). **(b)** July air temperature anomalies at Delta Sø, northwest Greenland, using two different training sets and transfer functions, FOR15 (light green) and FRA06 (dark green) (Axford et al., 2019). **(c)** Agassiz $\delta^{18}O$ temperature reconstruction (Lecavalier et al., 2017). **(d)** Reconstructed west Greenland sea surface temperatures from Gibb et al. (2015) (dark blue) and Ouellet-Bernier et al. (2014) (light blue). Panel **(e)** shows the inferred ice extent in north and northwest Greenland from Melville Bay in the south to Washington Land in the north (for references, see text). Dark red bars denote known periods of deglaciation from the outer coast towards the present-day ice margin and bright red bars denote periods of smaller than present-day extent. Arrows indicate the lack of an upper or lower constraint.

dating the LGM and an overall 89 % of the samples being affected by inheritance, possibly due to low-erosive cold-based ice. We find that the outer coast in Inglefield Land began to deglaciate between ca. 8.6 and 8.3 ka cal BP in the southeastern part, whereas the central part was deglaciated by ca. 7.9 ka. Following initial deglaciation, the ice margin reached its present-day position at ca. 6.7 ka in central Inglefield Land, whereas Humboldt Glacier in the northern part of the study area already reached its present-day extent by ca. 8.2 ka. After deglaciation, the ice margin retreated behind its present-day extent from ca. 5.8 to 1.9 ka cal BP at the Hiawatha Glacier and ca. 3.7 to 0.3 ka cal BP at the Humboldt Glacier. Thus, the re-advance towards the LIA extent was initiated between 1.9 and 0.3 ka cal BP.

We furthermore reviewed new data from northwest and north Greenland to put our results into a broader context and assessed the findings with local and regional climate records. We found that the Holocene glacial history varies significantly between northwest and north Greenland. The deglaciation from the coast to the present-day ice extent in northwest Greenland occurred at the onset of the Holocene, possibly as a response to the relatively early HTM. Deglaciation continued and the ice sheet retreated behind its present-day extent in northwest Greenland throughout most of the Middle and Late Holocene, driven by continued high air temperatures and the arrival of warm waters along the west Greenland coast. In contrast, the deglaciation of the outer coast in Nares Strait and north Greenland was delayed by ca. 2–3 kyr and shows a more restricted period of retreat behind its present-day extent. The observed difference in patterns of deglaciation in the two regions is most likely a consequence of the large marine-based part of the northwest GrIS being more sensitive to climate changes as opposed to the largely land-based north GrIS. Further, the late opening of Nares Strait could have delayed ice retreat in north Greenland, despite early atmospheric warming. During the LIA cooling, the GrIS do though show a synchronous response, with ice advance throughout northwest and north Greenland. Our findings highlight the complexity of the ice–climate system and show clear differences in ice sheet sensitivity between northwest and north Greenland. As such, this adds new knowledge and possible constraints on the future state of the GrIS as a response to present-day global warming.

Data availability. All analytical information for the cosmogenic-nuclide and radiocarbon measurements are available in the tables.

Author contributions. NKL, KHK, SF and ASS participated in fieldwork and decided on the sampling strategy. ASS did ^{10}Be sample preparation and JO and ASS carried out measurements and calculation. OS and ASS carried out in situ ^{14}C sample preparation, measurements and calculation. DLE and ASS carried out in situ ^{14}C modelling experiments. ASS and NKL made initial interpretations of the results and wrote the paper with contributions from the co-authors.

Competing interests. The authors declare that they have no conflict of interest.

Acknowledgements. We thank Birte Lindahl Eriksen and Rikke Brok Jensen for extensive help processing ^{10}Be and ^{26}Al samples.

Financial support. This research has been supported by the Villum Foundation (VRK 02344), Aarhus University Research Foundation, and the Carlsberg Foudation.

Review statement. This paper was edited by Irina Rogozhina and reviewed by Yarrow Axford and one anonymous referee.

References

Axford, Y., Lasher, G. E., Kelly, M. A., Osterberg, E. C., Landis, J., Schellinger, G. C., Pfeiffer, A., Thompson, E., and Francis, D. R.: Holocene temperature history of northwest Greenland – With new ice cap constraints and chironomid assemblages from Deltasø, Quaternary Sci. Rev., 215, 160–172, https://doi.org/10.1016/j.quascirev.2019.05.011, 2019.

Balco, G.: Glacier Change and Paleoclimate Applications of Cosmogenic-Nuclide Exposure Dating, Annu. Rev. Earth Pl. Sc., 48, 1.1–1.28, https://doi.org/10.1146/annurev-earth-081619-052609, 2020.

Balco, G., Stone, J. O., Lifton, N. A., and Dunai, T. J.: A complete and easily accessible means of calculating surface exposure ages or erosion rates from ^{10}Be and ^{26}Al measurements, Quat. Geochronol., 3, 174–195, https://doi.org/10.1016/j.quageo.2007.12.001, 2008.

Bennike, O.: Late Quaternary history of Washington Land, North Greenland, Boreas, 31, 260–272, 2002.

Bennike, O.: An early Holocene Greenland whale from Melville Bugt, Greenland, Quaternary Res., 69, 72–76, https://doi.org/10.1016/j.yqres.2007.10.004, 2008.

Bennike, O. and Björck, S.: Chronology of the last recession of the Greenland Ice Sheet, J. Quaternary Sci., 17, 211–219, https://doi.org/10.1002/jqs.670, 2002.

Bennike, O. and Weidick, A.: Late Quaternary history around Nioghalvfjerdsfjorden and Jøkelbugten, North-East Greenland, Boreas, 30, 205–227, 2001.

Blake, W., Boucherle, M. M., Fredskild, B., Janssens, J. A., and Smol, J. P.: The geomorphological setting, glacial history and Holocene developement of "Kap Inglefield Sø", Inglefield Land, North-West Greenland, Meddelelser om Grønland, Geoscience, 27, 42, 1992.

Briner, J. P., Håkansson, L., and Bennike, O.: The deglaciation and neoglaciation of Upernavik Isstrøm, Greenland, Quaternary Res., 80, 459–467, https://doi.org/10.1016/j.yqres.2013.09.008, 2013.

Briner, J. P., Kaufman, D. S., Bennike, O., and Kosnik, M. A.: Amino acid ratios in reworked marine bivalve shells constrain Greenland Ice Sheet history during the Holocene, Geology, 42, 75–78, https://doi.org/10.1130/g34843.1, 2014.

Briner, J. P., McKay, N. P., Axford, Y., Bennike, O., Bradley, R. S., de Vernal, A., Fisher, D., Francus, P., Fréchette, B., Gajewski, K., Jennings, A., Kaufman, D. S., Miller, G., Rouston, C., and Wagner, B.: Holocene climate change in Arctic Canada and Greenland, Quaternary Sci. Rev., 147, 340–364, https://doi.org/10.1016/j.quascirev.2016.02.010, 2016.

Brock, F., Higham, T., Ditchfield, P., and Ramsey, C. B.: Current Pretreatment Methods for AMS Radiocarbon Dating at the Oxford Radiocarbon Accelerator Unit (Orau), Radiocarbon, 52, 103–112, https://doi.org/10.1017/s0033822200045069, 2010.

Buizert, C., Keisling, B. A., Box, J. E., He, F., Carlson, A. E., Sinclair, G., and DeConto, R. M.: Greenland-Wide Seasonal Temperatures During the Last Deglaciation, Geophys. Res. Lett., 45, 1905–1914, https://doi.org/10.1002/2017gl075601, 2018.

Caron, M., Montero-Serrano, J. C., St-Onge, G., and Rochon, A.: Quantifying provenance and transport pathways of Holocene sediments from the northwestern Greenland margin, Paleoceanography and Paleoclimatology, 35, e2019PA003809, https://doi.org/10.1029/2019pa003809, 2020.

Ceperley, E. G., Marcott, S. A., Reusche, M. M., Barth, A. M., Mix, A. C., Brook, E. J., and Caffee, M.: Widespread early Holocene deglaciation, Washington Land, northwest Greenland, Quaternary Sci. Rev., 231, 106181, https://doi.org/10.1016/j.quascirev.2020.106181, 2020.

Corbett, L. B., Bierman, P. R., Graly, J. A., Neumann, T. A., and Rood, D. H.: Constraining landscape history and glacial erosivity using paired cosmogenic nuclides in Upernavik, northwest Greenland, Geol. Soc. Am. Bull., 125, 1539–1553, https://doi.org/10.1130/b30813.1, 2013.

Corbett, L. B., Bierman, P. R., Lasher, G. E., and Rood, D. H.: Landscape chronology and glacial history in Thule, northwest Greenland, Quaternary Sci. Rev., 109, 57–67, https://doi.org/10.1016/j.quascirev.2014.11.019, 2015.

Corbett, L. B., Bierman, P. R., and Rood, D. H.: An approach for optimizing in situ cosmogenic ^{10}Be sample preparation, Quat. Geochronol., 33, 24–34, https://doi.org/10.1016/j.quageo.2016.02.001, 2016.

Dalton, A. S., Margold, M., Stokes, C. R., Tarasov, L., Dyke, A. S., Adams, R. S., Allard, S., Arends, H. E., Atkinson, N., Attig, J. W., Barnett, P. J., Barnett, R. L., Batterson, M., Bernatchez, P., Borns, H. W., Breckenridge, A., Briner, J. P., Brouard, E., Campbell, J. E., Carlson, A. E., Clague, J. J., Curry, B. B., Daigneault, R.-A., Dubé-Loubert, H., Easterbrook, D. J., Franzi, D. A., Friedrich, H. G., Funder, S., Gauthier, M. S., Gowan, A. S., Harris, K. L., Hétu, B., Hooyer, T. S., Jennings, C. E., Johnson, M. D., Kehew, A. E., Kelley, S. E., Kerr, D., King, E. L., Kjeldsen, K. K., Knaeble, A. R., Lajeunesse, P., Lakeman, T. R., Lamothe, M., Larson, P., Lavoie, M., Loope, H. M., Lowell, T. V., Lusardi, B. A., Manz, L., McMartin, I., Nixon, F. C., Occhietti, S., Parkhill, M. A., Piper, D. J. W., Pronk, A. G., Richard, P. J. H., Ridge, J. C., Ross, M., Roy, M., Seaman, A., Shaw, J., Stea, R. R., Teller, J. T., Thompson, W. B., Thorleifson, L. H., Utting, D. J., Veillette, J. J., Ward, B. C., Weddle, T. K., and Wright, H. E.: An updated radiocarbon-based ice margin chronology for the last deglaciation of the North American Ice Sheet Complex, Quaternary Sci. Rev., 234, 106223, https://doi.org/10.1016/j.quascirev.2020.106223, 2020.

Dawes, P. R.: Explanatory notes to the Geological map of Greenland, 1 : 500 000, Humbolt Gletscher, Sheet 6, Geological Survey of Denmark and Greenland Map Series 1, Copenhagen, Denmark, 48 pp., 2004.

Dyke, A. S., Dale, J. E., and McNeely, R. N.: Marine Molluscs as Indicators of Environmental Change in Glaciated North America and Greenland During the Last 18 000 Years, Geogr. Phys. Quatern., 50, 125–184, https://doi.org/10.7202/033087ar, 1996.

England, J.: Coalescent Greenland and Innuitian ice during the Last Glacial Maximum: revising the Quaternary of the Canadian High Arctic, Quaternary Sci. Rev., 18, 421–446, 1999.

England, J., Atkinson, N., Bednarski, J., Dyke, A. S., Hodgson, D. A., and Ó Cofaigh, C.: The Innuitian Ice Sheet: configuration, dynamics and chronology, Quaternary Sci. Rev., 25, 689–703, https://doi.org/10.1016/j.quascirev.2005.08.007, 2006.

Farnsworth, L. B., Kelly, M. A., Bromley, G. R. M., Axford, Y., Osterberg, E. C., Howley, J. A., Jackson, M. S., and Zimmerman, S. R.: Holocene history of the Greenland Ice-Sheet margin in Northern Nunatarssuaq, Northwest Greenland, Arktos, 4, 10, https://doi.org/10.1007/s41063-018-0044-0, 2018.

Funder, S. and Hansen, L.: The Greenland ice sheet – a model for its culmination and decay during and after the last glacial maximum, B. Geol. Soc. Denmark, 42, 137–152, 1996.

Funder, S., Kjeldsen, K. K., Kjær, K. H., and Ó Cofaigh, C.: The Greenland Ice Sheet During the Past 300,000 Years: A Review, Developments in Quaternary Sciences, 15, 699–713, https://doi.org/10.1016/b978-0-444-53447-7.00050-7, 2011.

Garde, A. A., Søndergaard, A. S., Guvad, C., Dahl-Møller, J., Nehrke, G., Sanei, H., Weikusat, C., Funder, S., Kjær, K. H., and Larsen, N. K.: Pleistocene organic matter modified by the Hiawatha impact, northwest Greenland, Geology, 48, 867–871, https://doi.org/10.1130/g47432.1, 2020.

Georgiadis, E., Giraudeau, J., Martinez, P., Lajeunesse, P., St-Onge, G., Schmidt, S., and Massé, G.: Deglacial to post-glacial history of Nares Strait, Northwest Greenland: a marine perspective from Kane Basin, Clim. Past, 14, 1991–2010, https://doi.org/10.5194/cp-14-1991-2018, 2018.

Gibb, O. T., Steinhauer, S., Fréchette, B., De Vernal, A., and Hillaire-Marcel, C.: Diachronous evolution of sea surface conditions in the Labrador Sea and Baffin Bay since the last deglaciation, Holocene, 25, 1882–1897, 2015.

Goehring, B. M., Wilson, J., and Nichols, K.: A fully automated system for the extraction of in situ cosmogenic carbon-14 in the Tulane University cosmogenic nuclide laboratory, Nucl. Instrum. Meth. B, 455, 284–292, https://doi.org/10.1016/j.nimb.2019.02.006, 2019.

Gosse, J. C. and Phillips, F. M.: Terrestrial in situ cosmogenic nuclides: theory and application, Quaternary Sci. Rev., 20, 1475–1560, 2001.

Graham, B. L., Briner, J. P., Schweinsberg, A. D., Lifton, N. A., and Bennike, O.: New in situ ^{14}C data indicate the absence of nunataks in west Greenland during the Last Glacial Maximum, Quaternary Sci. Rev., 225, 105981, https://doi.org/10.1016/j.quascirev.2019.105981, 2019.

Håkansson, L., Graf, A., Strasky, S., Ivy-ochs, S., Kubik, P. W., Hjort, C., and Schlüchter, C.: Cosmogenic ^{10}Be-ages from the store koldewey island, ne greenland, Geogr. Ann. A, 89, 195–202, https://doi.org/10.1111/j.1468-0459.2007.00318.x, 2016.

Heyman, J., Stroeven, A. P., Harbor, J. M., and Caffee, M. W.: Too young or too old: Evaluating cosmogenic exposure dating based on an analysis of compiled boulder exposure ages, Earth Planet. Sc. Lett., 302, 71–80, https://doi.org/10.1016/j.epsl.2010.11.040, 2011.

Hill, E. A., Carr, J. R., and Stokes, C. R.: A Review of Recent Changes in Major Marine-Terminating Outlet Glaciers in Northern Greenland, Front. Earth Sci., 4, 111, https://doi.org/10.3389/feart.2016.00111, 2017.

Hippe, K.: Constraining processes of landscape change with combined in situ cosmogenic ^{14}C-^{10}Be analysis, Quaternary Sci. Rev., 173, 1–19, https://doi.org/10.1016/j.quascirev.2017.07.020, 2017.

Hippe, K. and Lifton, N. A.: Calculating Isotope Ratios and Nuclide Concentrations for In Situ Cosmogenic ^{14}C Analyses, Radiocarbon, 56, 1167–1174, https://doi.org/10.2458/56.17917, 2016.

Hippe, K., Kober, F., Baur, H., Ruff, M., Wacker, L., and Wieler, R.: The current performance of the in situ ^{14}C extraction line at ETH, Quat. Geochronol., 4, 493–500, https://doi.org/10.1016/j.quageo.2009.06.001, 2009.

Ivy-Ochs, S. and Kober, F.: Surface exposure dating with cosmogenic nuclides, Quaternary Sci. J., 57, 179–209, 2008.

Jakobsson, M., Hogan, K. A., Mayer, L. A., Mix, A., Jennings, A., Stoner, J., Eriksson, B., Jerram, K., Mohammad, R., Pearce, C., Reilly, B., and Stranne, C.: The Holocene retreat dynamics and stability of Petermann Glacier in northwest Greenland, Nat. Commun., 9, 2104, https://doi.org/10.1038/s41467-018-04573-2, 2018.

Jennings, A. E., Sheldon, C., Cronin, T. M., Francus, P., Stoner, J., and Andrews, J.: The Holocene history of Nares Strait: Transition from Glacial Bay to Arctic-Atlamntic Throughflow, Oceanography, 24, 27–41, 2011.

Jennings, A. E., Andrews, J. T., Oliver, B., Walczak, M., and Mix, A.: Retreat of the Smith Sound Ice Stream in the Early Holocene, Boreas, 48, 825–840, https://doi.org/10.1111/bor.12391, 2019.

Kelly, M. A., Lowell, T. V., Hall, B. L., Schaefer, J. M., Finkel, R. C., Goehring, B. M., Alley, R. B., and Denton, G. H.: A ^{10}Be chronology of lateglacial and Holocene mountain glaciation in the Scoresby Sund region, east Greenland: implications for seasonality during lateglacial time, Quaternary Sci. Rev., 27, 2273–2282, https://doi.org/10.1016/j.quascirev.2008.08.004, 2008.

Khan, S. A., Aschwanden, A., Bjork, A. A., Wahr, J., Kjeldsen, K. K., and Kjaer, K. H.: Greenland ice sheet mass balance: a review, Rep. Prog. Phys., 78, 046801, https://doi.org/10.1088/0034-4885/78/4/046801, 2015.

Kjær, K. H., Larsen, N. K., Binder, T., Bjørk, A. A., Eisen, O., Fahnestock, M. A., Funder, S., Garde, A. A., Haack, H., Helm, V., Houmark-Nielsen, M., Kjeldsen, K. K., Khan, S. A., Machguth, H., McDonald, I., Morlighem, M., Mouginot, J., Paden, J. D., Waight, T. E., Weikusat, C., Willerslev, E., and MacGreor, J. A.: A large impact crater beneath Hiawatha Glacier in northwest Greenland, Sci. Adv., 4, 1–11, 2018.

Kolb, J., Keiding, J. K., Steenfelt, A., Secher, K., Keulen, N., Rosa, D., and Stensgaard, B. M.: Metallogeny of Greenland, Ore Geol. Rev., 78, 493–555, https://doi.org/10.1016/j.oregeorev.2016.03.006, 2016.

Lal, D.: Cosmic ray labeling of erosion surface: in situ nuclide production rates and erosion models, Earth Planet. Sc. Lett., 104, 424–439, 1991.

Larsen, N. K., Funder, S., Kjær, K. H., Kjeldsen, K. K., Knudsen, M. F., and Linge, H.: Rapid early Holocene ice retreat in West Greenland, Quaternary Sci. Rev., 92, 310–323, https://doi.org/10.1016/j.quascirev.2013.05.027, 2014.

Larsen, N. K., Levy, L. B., Carlson, A. E., Buizert, C., Olsen, J., Strunk, A., Bjork, A. A., and Skov, D. S.: Instability of the Northeast Greenland Ice Stream over the last 45,000 years, Nat. Commun., 9, 1872, https://doi.org/10.1038/s41467-018-04312-7, 2018.

Larsen, N. K., Levy, L. B., Strunk, A., Søndergaard, A. S., Olsen, J., and Lauridsen, T. L.: Local ice caps in Finderup Land, North

Greenland, survived the Holocene Thermal Maximum, Boreas, 48, 551–562, https://doi.org/10.1111/bor.12384, 2019.

Larsen, N. K., Søndergaard, A. S., Levy, L. B., Olsen, J., Strunk, A., Bjørk, A. A., and Skov, D. S.: Contrasting modes of delaciation between fjords and inter-fjord areas in eastern North Greenland, Boreas, 12475, https://doi.org/10.1111/bor.12475, online first, 2020.

Lasher, G. E., Axford, Y., McFarlin, J. M., Kelly, M. A., Osterberg, E. C., and Berkelhammer, M. B.: Holocene temperatures and isotopes of precipitation in Northwest Greenland recorded in lacustrine organic materials, Quaternary Sci. Rev., 170, 45–55, https://doi.org/10.1016/j.quascirev.2017.06.016, 2017.

Lecavalier, B. S., Fisher, D. A., Milne, G. A., Vinther, B. M., Tarasov, L., Huybrechts, P., Lacelle, D., Main, B., Zheng, J., Bourgeois, J., and Dyke, A. S.: High Arctic Holocene temperature record from the Agassiz ice cap and Greenland ice sheet evolution, P. Natl. Acad. Sci. USA, 114, 5952–5957, https://doi.org/10.1073/pnas.1616287114, 2017.

Levac, E., Vernal, A. D., and Blake Jr, W.: Sea-surface conditions in northernmost Baffin Bay during the Holocene: palynological evidence, J. Quaternary Sci., 16, 353–363, https://doi.org/10.1002/jqs.614, 2001.

Lifton, N. A., Jull, A. J. T., and Quade, J.: A new extraction technique and production rate estimate for in situ cosmogenic ^{14}C in quartz, Geochim. Cosmochim. Ac., 65, 1953–1969, 2001.

Lifton, N., Goehring, B., Wilson, J., Kubley, T., and Caffee, M.: Progress in automated extraction and purification of in situ ^{14}C from quartz: Results from the Purdue in situ ^{14}C laboratory, Nucl. Instrum. Meth. B, 361, 381–386, https://doi.org/10.1016/j.nimb.2015.03.028, 2015.

Livingstone, S. J., Chu, W., Ely, J. C., and Kingslake, J.: Paleofluvial and subglacial channel networks beneath Humboldt Glacier, Greenland, Geology, 45, 551–554, https://doi.org/10.1130/g38860.1, 2017.

Lupker, M., Hippe, K., Wacker, L., Steinemann, O., Tikhomirov, D., Maden, C., Haghipour, N., and Synal, H.-A.: In situ cosmogenic ^{14}C analysis at ETH Zürich: Characterization and performance of a new extraction system, Nucl. Instrum. Meth. B, 457, 30–36, https://doi.org/10.1016/j.nimb.2019.07.028, 2019.

MacGregor, J. A., Fahnestock, M. A., Catania, G. A., Aschwanden, A., Clow, G. D., Colgan, W. T., Gogineni, S. P., Morlighem, M., Nowicki, S. M. J., Paden, J. D., Price, S. F., and Seroussi, H.: A synthesis of the basal thermal state of the Greenland Ice Sheet, J. Geophys. Res.-Earth, 121, 1328–1350, https://doi.org/10.1002/2015JF003803, 2016.

Mason, O. K.: Beach Ridge Geomorphology at Cape Grinnell, northern Greenland: A Less Icy Arctic in the Mid-Holocene, Danish Journal of Geography, 110, 337–355, 2010.

McFarlin, J. M., Axford, Y., Osburn, M. R., Kelly, M. A., Osterberg, E. C., and Farnsworth, L. B.: Pronounced summer warming in northwest Greenland during the Holocene and Last Interglacial, P. Natl. Acad. Sci. USA, 115, 6357–6362, https://doi.org/10.1073/pnas.1720420115, 2018.

Morlighem, M., Rignot, E., Mouginot, J., Seroussi, H., and Larour, E.: Deeply incised submarine glacial valleys beneath the Greenland ice sheet, Nat. Geosci., 7, 418–422, https://doi.org/10.1038/ngeo2167, 2014.

Morlighem, M., Williams, C. N., Rignot, E., An, L., Arndt, J. E., Bamber, J. L., Catania, G., Chauche, N., Dowdeswell, J. A., Dorschel, B., Fenty, I., Hogan, K., Howat, I., Hubbard, A., Jakobsson, M., Jordan, T. M., Kjeldsen, K. K., Millan, R., Mayer, L., Mouginot, J., Noel, B. P. Y., O'Cofaigh, C., Palmer, S., Rysgaard, S., Seroussi, H., Siegert, M. J., Slabon, P., Straneo, F., van den Broeke, M. R., Weinrebe, W., Wood, M., and Zinglersen, K. B.: BedMachine v3: Complete Bed Topography and Ocean Bathymetry Mapping of Greenland From Multibeam Echo Sounding Combined With Mass Conservation, Geophys. Res. Lett., 44, 11051–11061, https://doi.org/10.1002/2017GL074954, 2017.

Mörner, N. A. and Funder, S. V.: C-14 dating of samples collected during the NORDQUA 86 expedition, and notes on the marine reservoir effect, Meddelelser om Grønland, 22, 57–59, 1990.

Mouginot, J., Rignot, E., Bjork, A. A., van den Broeke, M., Millan, R., Morlighem, M., Noel, B., Scheuchl, B., and Wood, M.: Forty-six years of Greenland Ice Sheet mass balance from 1972 to 2018, P. Natl. Acad. Sci. USA, 116, 9239–9244, https://doi.org/10.1073/pnas.1904242116, 2019.

Nichols, R., L: Geomorphology of Inglefield Land, North Greenland, Meddelelser om Grønland, 188, 109 pp., 1969.

Nishiizumi, K., Imamura, M., Caffee, M. W., Southon, J. R., Finkel, R. C., and McAninch, J.: Absolute calibration of ^{10}Be AMS standards, Nucl. Instrum. Meth. B, 258, 403–413, https://doi.org/10.1016/j.nimb.2007.01.297, 2007.

Noël, B., van de Berg, W. J., Lhermitte, S., and van der Broeke, M. R.: Rapid ablation zone expansion amplifies north Greenland mass loss, Sci. Adva., 5, eaaw0123, https://doi.org/10.1126/sciadv.aaw0123, 2019.

Olsen, J., Tikhomirov, D., Grosen, C., Heinemeier, J., and Klein, M.: Radiocarbon Analysis on the New AARAMS 1MV Tandetron, Radiocarbon, 59, 905–913, https://doi.org/10.1017/rdc.2016.85, 2016.

Ouellet-Bernier, M.-M., De Vernal, A., Hillaire-Marcel, C., and Moros, M.: Paleoceanographic changes in the Disko Bugt area, West Greenland, during the Holocene, Holocene, 24, 1573–1583, 2014.

Ramsey, B. C.: Bayesian Analysis of Radiocarbon Dates, Radiocarbon, 51, 337–360, https://doi.org/10.1017/S0033822200033865, 2009.

Reilly, B. T., Stoner, J. S., Mix, A. C., Walczak, M. H., Jennings, A., Jakobsson, M., Dyke, L., Glueder, A., Nicholls, K., Hogan, K. A., Mayer, L. A., Hatfield, R. G., Albert, S., Marcott, S., Fallon, S., and Cheseby, M.: Holocene break-up and reestablishment of the Petermann Ice Tongue, Northwest Greenland, Quaternary Sci. Rev., 218, 322–342, https://doi.org/10.1016/j.quascirev.2019.06.023, 2019.

Reimer, J. P., Bard, E., Bayliss, A., Beck, J. W., Blackwell, P. G., Ramsey, C. B., Buck, C. E., Cheng, H., Edwards, R. L., Friedrich, M., Grootes, P. M., Guilderson, T. P., Haflidason, H., Hajdas, I., Hatté, C., Heaton, T. J., Hoffmann, D. L., Hogg, A. G., Hughen, K. A., Kaiser, K. F., Kromer, B., Manning, S. W., Niu, M., Reimer, R. W., Richards, D. A., Scott, E. M., Southon, J. R., Staff, R. A., Turney, C. S. M., and van der Plicht, J.: Intcal13 and Marine13 radiocarbon age calibration curves 0–50,000 years cal BP, Radiocarbon, 4, 1869–1887, 2013.

Reusche, M. M., Marcott, S. A., Ceperley, E. G., Barth, A. M., Brook, E. J., Mix, A. C., and Caffee, M. W.: Early to Late Holocene Surface Exposure Ages From Two Marine-Terminating Outlet Glaciers in North-

west Greenland, Geophys. Res. Lett., 45, 7028–7039, https://doi.org/10.1029/2018gl078266, 2018.

Rignot, E. and Kanagaratnam, P.: Changes in the Velocity Structure of the Greenland Ice Sheet, Science, 311, 986–990, 2006.

Sinclair, G., Carlson, A. E., Mix, A. C., Lecavalier, B. S., Milne, G., Mathias, A., Buizert, C., and DeConto, R.: Diachronous retreat of the Greenland ice sheet during the last deglaciation, Quaternary Sci. Rev., 145, 243–258, https://doi.org/10.1016/j.quascirev.2016.05.040, 2016.

Skov, D. S., Egholm, D. L., Larsen, N. K., Jansen, J. D., Knudsen, M. F., Jacobsen, B. H., Olsen, J., and Andersen, J. L.: Constraints from cosmogenic nuclides on the glaciation and erosion history of Dove Bugt, northeast Greenland, GSA Bulletin, B35410.1, https://doi.org/10.1130/b35410.1, online first, 2020.

Søndergaard, A. S., Larsen, N. K., Olsen, J., Strunk, A., and Woodroffe, S.: Glacial history of the Greenland Ice Sheet and a local ice cap in Qaanaaq, northwest Greenland, J. Quaternary Sci., 34, 536–547, https://doi.org/10.1002/jqs.3139, 2019.

Søndergaard, A. S., Larsen, N. K., Lecavalier, B. S., Olsen, J., Fitzpatrick, N. P., Kjær, K. H., and Khan, S. A.: Early Holocene collapse of marine-based ice in northwest Greenland triggered by atmospheric warming, Quaternary Sci. Rev., 239, 106360, https://doi.org/10.1016/j.quascirev.2020.106360, 2020.

Stone, J. O.: Air pressure and cosmogenic isotope production, J. Geophys. Res.-Sol. Ea., 105, 23753–23759, https://doi.org/10.1029/2000jb900181, 2000.

Synal, H.-A., Stocker, M., and Suter, M.: MICADAS: A new compact radiocarbon AMS system, Nucl. Instrum. Meth. B, 259, 7–13, https://doi.org/10.1016/j.nimb.2007.01.138, 2007.

Tedrow, J. C. F.: Soil investigation in Inglefield Land, Greenland, Meddelelser om Grønland, 188, 94 pp., 1970.

Wacker, L., Bonani, G., Friedrich, M., Hajdas, I., Kromer, B., Němec, M., Ruff, M., Suter, M., Synal, H. A., and Vockenhuber, C.: MICADAS: Routine and High-Precision Radiocarbon Dating, Radiocarbon, 52, 252–262, https://doi.org/10.1017/s0033822200045288, 2010.

Young, N. E., Briner, J. P., Rood, D. H., Finkel, R. C., Corbett, L. B., and Bierman, P. R.: Age of the Fjord Stade moraines in the Disko Bugt region, western Greenland, and the 9.3 and 8.2 ka cooling events, Quaternary Sci. Rev., 60, 76–90, https://doi.org/10.1016/j.quascirev.2012.09.028, 2012.

Young, N. E., Schaefer, J. M., Briner, J. P., and Goehring, B. M.: A ^{10}Be production-rate calibration for the Arctic, J. Quaternary Sci., 28, 515–526, https://doi.org/10.1002/jqs.2642, 2013.

Young, N. E., Schaefer, J. M., Goehring, B., Lifton, N., Schimmelpfennig, I., and Briner, J. P.: West Greenland and globalin situ ^{14}C production-rate calibrations, J. Quaternary Sci., 29, 401–406, https://doi.org/10.1002/jqs.2717, 2014.

Young, N. E., Lamp, J., Koffman, T., Briner, J. P., Schaefer, J., Gjermundsen, E. F., Linge, H., Zimmerman, S., Guilderson, T. P., Fabel, D., and Hormes, A.: Deglaciation of coastal south-western Spitsbergen dated with in situ cosmogenic ^{10}Be and ^{14}C measurements, J. Quaternary Sci., 33, 763–776, https://doi.org/10.1002/jqs.3058, 2018.

Young, N. E., Briner, J. P., Miller, G. H., Lesnek, A. J., Crump, S. E., Thomas, E. K., Pendleton, S. L., Cuzzone, J., Lamp, J., Zimmerman, S., Caffee, M., and Schaefer, J. M.: Deglaciation of the Greenland and Laurentide ice sheets interrupted by glacier advance during abrupt coolings, Quaternary Sci. Rev., 229, 106091, https://doi.org/10.1016/j.quascirev.2019.106091, 2020.